

RESEARCH ARTICLE

L-Type Calcium Channel Inhibition Contributes to the Proarrhythmic Effects of Aconitine in Human Cardiomyocytes

Jianjun Wu¹, Xiangchong Wang², Ying Ying Chung¹, Cai Hong Koh¹, Zhenfeng Liu¹, Huicai Guo³, Qiang Yuan⁴, Chuan Wang², Suwen Su^{2*}, Heming Wei^{1,5*}

1 National Heart Research Institute Singapore, National Heart Centre Singapore, Singapore, **2** Department of Pharmacology, Hebei Medical University, Shijiazhuang, Hebei, China, **3** Department of Toxicology, Hebei Medical University, Shijiazhuang, Hebei, China, **4** Neuroscience & Behavioral Disorders Program, Duke-NUS Medical School Singapore, Singapore, **5** Cardiovascular & Metabolic Disorders Program, Duke-NUS Medical School Singapore, Singapore

* wei.he.ming@nhcs.com.sg (HW); suswmk@hebmh.edu.cn (SS)



OPEN ACCESS

Citation: Wu J, Wang X, Chung YY, Koh CH, Liu Z, Guo H, et al. (2017) L-Type Calcium Channel Inhibition Contributes to the Proarrhythmic Effects of Aconitine in Human Cardiomyocytes. PLoS ONE 12(1): e0168435. doi:10.1371/journal.pone.0168435

Editor: Alexander G. Obukhov, Indiana University School of Medicine, UNITED STATES

Received: June 1, 2016

Accepted: December 1, 2016

Published: January 5, 2017

Copyright: © 2017 Wu et al. This is an open access article distributed under the terms of the [Creative Commons Attribution License](https://creativecommons.org/licenses/by/4.0/), which permits unrestricted use, distribution, and reproduction in any medium, provided the original author and source are credited.

Data Availability Statement: All relevant data are within the paper and its Supporting Information files.

Funding: This work was supported by: National Medical Research Council, NMRC CG12Aug09, Dr Heming Wei; Duke-NUS GOH Cardiovascular Research Award, GCR/2012/0006, Dr Heming Wei; National Natural Science Foundation of China, NSFC, 81273600, Suwen Su; Natural Science Foundation of Hebei Province, C2011206145, H2013206147, Suwen Su; National Natural Science

Abstract

Aconitine (ACO) is well-known for causing lethal ventricular tachyarrhythmias. While cardiac Na⁺ channel opening during repolarization has long been documented in animal cardiac myocytes, the cellular effects and mechanism of ACO in human remain unexplored. This study aimed to assess the proarrhythmic effects of ACO in human induced pluripotent stem cell-derived cardiomyocytes (hiPSC-CMs). ACO concentration-dependently (0.3 ~ 3.0 μM) shortened the action potentials (AP) durations (APD) in ventricular-like hiPSC-CMs by > 40% and induced delayed after-depolarization. Laser-scanning confocal calcium imaging analysis showed that ACO decreased the duration and amplitude of [Ca²⁺]_i transients and increased in the beating frequencies by over 60%. Moreover, ACO was found to markedly reduce the L-type calcium channel (LTCC) currents (I_{Ca,L}) in hiPSC-CMs associated with a positive-shift of activation and a negative shift of inactivation. ACO failed to alter the peak and late Na⁺ currents (I_{Na}) in hiPSC-CMs while it drastically increased the late I_{Na} in Guinea-pig ventricular myocytes associated with enhanced activation/delayed inactivation of I_{Na} at -55 mV ~ -85 mV. Further, the effects of ACO on I_{Ca,L}, I_{Na} and the rapid delayed rectifier potassium current (I_{Kr}) were validated in heterologous expression systems by automated voltage-clamping assays and a moderate suppression of I_{Kr} was observed in addition to concentration-dependent I_{Ca,L} inhibition. Lastly, increased beating frequency, decreased Ca²⁺ wave and shortened field potential duration were recorded from hiPSC-CMs by microelectrode arrays assay. In summary, our data demonstrated that LTCC inhibition could play a main role in the proarrhythmic action of ACO in human cardiomyocytes.

Introduction

Aconitum is a well-known medical herb which has been used world widely for over 2000 years. However, aconitine (ACO), the main effective ingredient of aconitum and a highly

Foundation of China, No. 81273600, 31171097, Dr Chuan Wang; and the Natural Science Foundation of Hebei Province, China, No. C2011206145, C2014206419, Dr Chuan Wang. The funders had no role in study design, data collection and analysis, decision to publish, or preparation of the manuscript.

Competing Interests: The authors have declared that no competing interests exist.

toxic diterpenoid alkaloid, has long been associated with severe cardiovascular toxicities including tachyarrhythmia and hypotension that causes a high mortality in patients [1,2].

Previous studies indicate that ACO is capable of inducing ventricular tachycardia (VT) and ventricular fibrillation (VF) in mouse [3], rat [4], Guinea-pig [5] and rabbits [6]. In isolated sheep heart Purkinje fibers, ACO has been shown to act as a cardiac Na^+ channel agonist that opens the Na^+ channels during the depolarization/repolarization phase of an action potentials (AP), leading to a delayed repolarization and early after-depolarization [7]. Similar effects of ACO were found in isolated ventricular myocytes of mice [8] and rats [9] and potentially in Guinea-pigs as well [10].

In addition, ACO-induced L-type Calcium channel (LTCC) inhibition has been observed in neonatal [11] and isolated adult [12] rat cardiac myocytes. Accumulated intracellular Na^+ has been recognized for activating the reverse-mode of Na^+ - Ca^{2+} exchanger (NCX) and increasing cytosolic $[\text{Ca}^{2+}]_i$, which can trigger intercellular $[\text{Ca}^{2+}]_i$ concentration dependent inactivation (CDI) of the LTCC [13,14]. It remains unclear if LTCC inhibition by ACO is due to accumulation of $[\text{Na}^+]_i$.

There are other possible mechanisms involved in ACO-induced toxicity. ACO has also been found capable of blocking the $\text{Kv}1.5$ channels that mediate the outward ultra-rapidly activating delayed rectifier K^+ current (I_{Kur}) in neonatal rat ventricular myocytes [15,16] while studies also demonstrated that ACO inhibited hERG in *Xenopus laevis* oocytes [16] and HEK293 cells [17].

Despite many intoxication incidences occurred each year, the proarrhythmic effects of ACO in human and the underlying mechanism remain unexplored due to a lack of human cardiomyocyte models. The recent scientific breakthrough has enabled the generation of human induced pluripotent stem cells (hiPSCs)-derived cardiomyocytes (hiPSC-CMs) which share important structural and functional similarities with native human cardiac myocytes. To date, hiPSC-CMs have been successfully adopted for modeling various cardiac diseases [18,19] and for drug testing [20,21].

We hypothesize that ACO-induced arrhythmia in human may involve an alternative mechanism different from that observed in animals due to a marked inter-species variation in cardiac electrophysiology [22,23].

In the present studies, we showed that ACO is able to block the $I_{\text{Ca,L}}$ and calcium-induced calcium release (CICR) in hiPSC-CMs without altering I_{Na} . Such effects could contribute to the shortened repolarization period characterized by shortened AP duration (APD) and field potential duration (FPDc).

Materials and Methods

Chemicals and drugs

ACO, Bay K-8644, and nifedipine were obtained from Sigma-Aldrich (St. Louis, USA). Tetrodotoxin (TTX) was obtained from Aik Moh (Singapore). The stock solutions of ACO (25 mM), Bay K-8644 (1 mM) and nifedipine (1 mM) were prepared in ethanol and stored at 4°C. The stock solution of TTX (5 mM) was prepared in extracellular solution and stored at -80°C.

Conventional patch-clamp recordings of cardiomyocytes

Cardiomyocytes used in this study were hiPSC-CMs purchased from Cellular Dynamics International Inc (Madison, USA). Cells were maintained at 37°C in a humidified CO_2 (5%) incubator in maintenance medium provided by the company.

Whole cell configuration of the patch-clamp technique was used to measure action potentials (AP) and calcium and sodium currents. The signal was amplified using an Axon 700B

patch-clamp amplifier (Axon Instrument, Sunnyvale, USA) and low-pass filtered at 5 kHz. Patch pipettes were fabricated from glass capillaries (O.D, 1.5mm; I.D, 0.9mm) using a Sutter P-97 microelectrode puller (Novato, CA, USA) and the tips were heat polished with a microforge (NARISHIGE MF-900) to gain a resistance of 2–4 M Ω . The electrical signals were sampled at 2.5–10 kHz and filtered at 2 kHz using a low-pass filter. Data acquisition was achieved using the Digidata 1440A (Axon Instrument). Data analysis and fit were performed using clamp fit 10.2 (Axon Instrument) and Origin 7.0 software (Origin Lab Corporation). A pClamp software (Version 8.1; Axon Instrument) was used to generate voltage-pulse protocols, acquire and analyze data.

Action potential recordings in hiPSC-CMs. The APs were recorded under current-clamp mode in normal Tyrode's solution contained (in mM): NaCl 140, KCl 5.4, CaCl₂ 1.8, MgCl₂ 1, glucose 10, and HEPES 10, adjusted to pH 7.4 with NaOH. Pipette solution contained (in mM): KCl 130, NaCl 5, MgCl₂ 1, MgATP 3, EGTA 10, and HEPES 10, adjusted to pH 7.2 with KOH. The parameters of APs include AP durations (APD) at 30%, 50% and 90% of repolarization (APD₃₀, APD₅₀, and APD₉₀), AP amplitude (APA), maximal diastolic potential (MDP), maximal upstroke velocity (dV/dt_{Max}) and beating frequency (BF) were analyzed [18,19]. The APDs were corrected by heart rates with Fridericia's formula (APD_c = APD/inter-spike interval^{1/3}) [24]. Cells were maintained at 35°C by a temperature controller (Warner Instruments, Hamden, USA) during the recording of action potential.

L-type calcium current (I_{Ca,L}) recording in hiPSC-CMs. Patch pipette solution contained (in mM): CsCl 120, MgCl₂ 3, MgATP 5, EGTA 10, and HEPES 5, adjusted to pH 7.2 with CsOH. External solution contained (in mM): NaCl 140, CsCl 10, CaCl₂ 1.8, MgCl₂ 1, glucose 10, and HEPES 10, adjusted to pH 7.4 with NaOH. To eliminate the 'run-down' effect during I_{Ca,L} recordings, Ba²⁺ was also used in the external solution (BaCl₂ 1.8 mM) to replace Ca²⁺ as charge carrier of calcium channel current [25]. Current-Voltage curve were generated by voltage-clamp protocols consisting of V_{hold} = -80 mV followed by a 3s long pre-pulse at -50 mV to inactivate Na⁺ and T-type Ca²⁺ channels, then a family of 300 ms depolarization from -50 mV to 50 mV in 10 mV increments.

Calcium channel current densities were obtained by dividing current amplitudes by membrane capacitances. Steady state (SS) inactivation variables of I_{Ca,L} were determined using a two-pulse gapped protocol. Potential was held at -40 mV, then pulsed to a conditioning pre-pulse ranging from -80mV to +10mV for 2000 ms, returned to -40 mV for 10 ms, and stepped to 0 mV for 250 ms at 10 s intervals. Voltage-dependence of activation curve and SS-inactivation curve were fitted with Boltzman equation ($G = G_{max} \times [1 + \exp((V_{1/2} - V)/\kappa)]^{-1}$), where G is the conductance at various test potentials and was calculated from the peak current according to $G = I/(V - V_{rev})$, V_{rev} is the reversal potential obtained by extrapolating the linear part of the I/V curve to its intersection with the voltage axis. G_{max} is maximum conductance; V_{1/2} and κ are half-activation voltage and the slope factor. The concentration-response data were fitted with Hill equation: $I/I_{max} = 1/[1 + (D/IC_{50})^n]$, where I is the peak current in various concentrations of compound, I_{max} is the maximal peak current, D is the compound concentration, IC₅₀ is the drug concentration for 50% inhibition, and n is the Hill coefficient.

The time course of recovery from inactivation of I_{Ca,L} was studied using a two-pulse protocol: a 250-ms pre-pulse (P1) at 0 mV from the holding potential of -50 mV followed by a variable recovery period and a 250-ms test pulse (P2) at 0 mV to assess the amount of current recovered. Each two-pulse sequence was separated by a 30 s interval. The time course of recovery for I_{Ca,L} was determined by fitting the data points to a single exponential function: $I/I_{max} = 1 - \exp(-t/\tau)$, where I_{max} and I were the peak current at pre-pulse (P1) and test pulse (P2), respectively; t was the variable recovery time; τ was the recovery time constant.

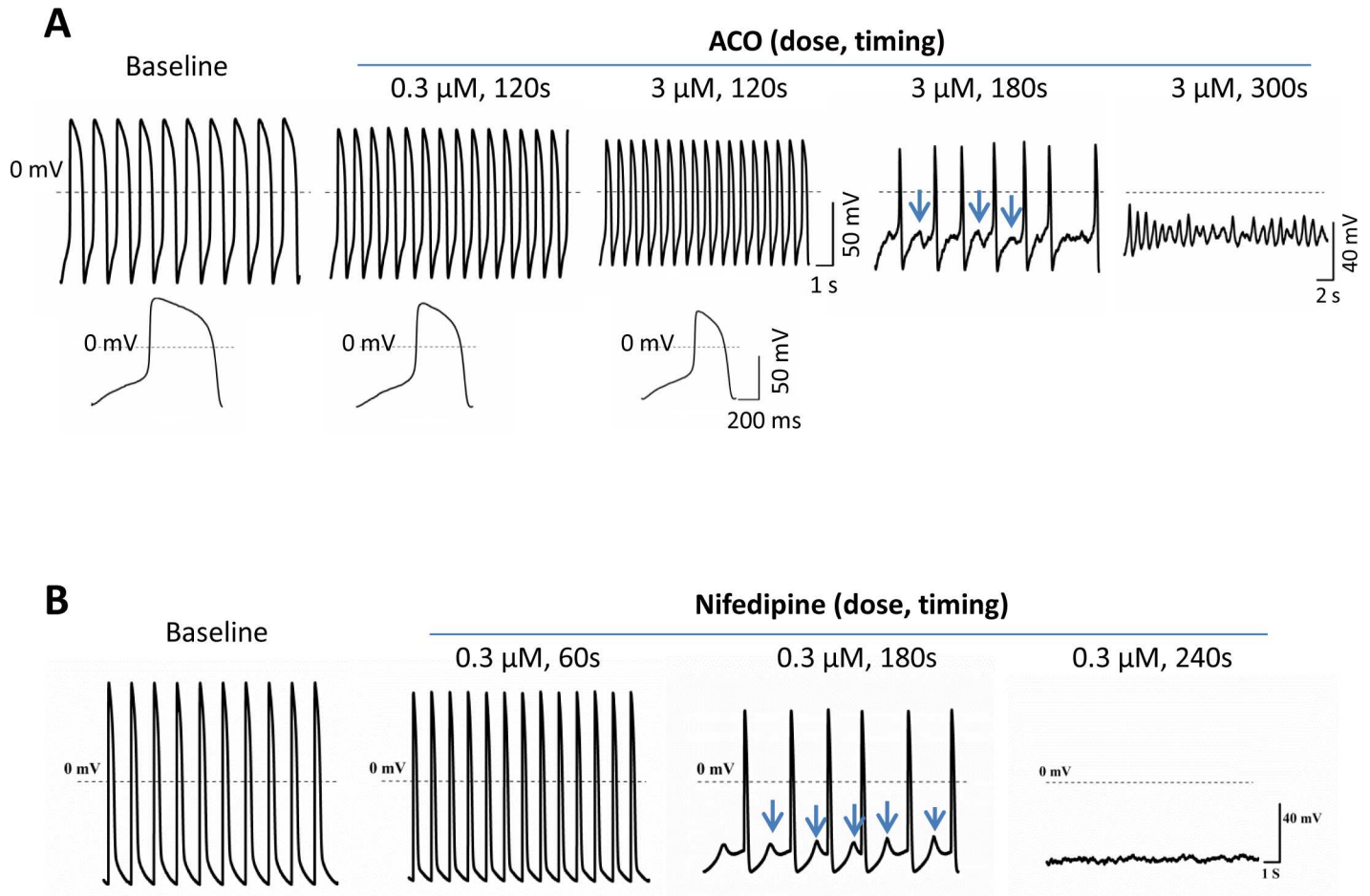


Fig 1. Effects of ACO on action potentials of hiPSC-CMs. (A) Representative AP waveforms recorded in a hiPSC-CM with 120 seconds (s) exposure of ACO at 0.3 and 3.0 μ M and 180s and 300s exposure of ACO at 3.0 μ M. Increased beating frequencies and decreased APD and APA were observed with short-term (120s) ACO treatment. Prolonged treatment of ACO at 3.0 μ M led to frequent DADs and rapid irregular VF-like AP changes. (B), Representative AP waveforms recorded in a hiPSC-CM exposed to 0.3 μ M nifedipine for 60s ~ 240s. Increased beating frequencies and decreased APD occurred at 60s while DADs emerged at 180s. APs were suppressed at 240s. The arrows indicate DADs.

doi:10.1371/journal.pone.0168435.g001

Peak and late sodium current (I_{Na} and I_{NaL}) recording in hiPSC-CMs and Guinea-pig ventricular myocytes. See [S1 File](#) (Supplemental Methods).

I_{Na} , I_{Kr} and $I_{Ca,L}$ recording in the heterologous expression systems by automated patch-clamping technique

See [S1 File](#) (Supplemental Methods) [26].

Laser-scanning confocal calcium imaging

$[Ca^{2+}]_i$ transients were recorded in hiPSC-CMs using a LSM-710 laser-scanning confocal microscope (Carl Zeiss, Inc, Germany) with a 40 \times , 1.3 numerical aperture oil immersion objective and axial resolutions of 1.5 μ m. Briefly, hiPSC-CMs were loaded with 2 μ M Fluo-8 AM (AAT Bioquest, Inc. Sunnyvale, CA, USA) for 15 min at 37 $^{\circ}$ C, and recorded in normal Tyrode's solution. Fluo-8 was excited at 488 nm, and fluorescence emission was measured at 505 nm. Images were acquired in the line-scan (X-T) mode with 512 pixels (pixel intervals of

0.15 μm) per line at a rate of 3 ms per scan. The $[\text{Ca}^{2+}]_i$ transients were analyzed using a modified version of MATLAB program. The Ca^{2+} fluorescence emission intensity was expressed as F/F_0 where the F_0 was the basal fluorescence intensity level. The recording was performed at 35°C temperature.

The microelectrode arrays (MEA) assay on hiPSC-CMs

See [S1 File](#) (Supplemental Methods) [24].

Statistical analysis

Values presented are means \pm standard error of means (SEM) for electrophysiology assays and means \pm standard derivation (SD) for calcium imaging assay. Statistical comparisons were made using Student’s unpaired or paired *t*-test. A value of $p < 0.05$ was considered statistically significant.

Results

The current study adopted concentrations of ACO ranged from 0.03 to 3 μM which is consistent with that (0.1 ~10 μM) adopted in the previous in vitro studies [7~10] and it covered the blood concentrations (0.02 ~ 0.11 μM) identified in patients with ACO-induced lethal cardiac arrhythmia [27].

Effects of ACO on APs of hiPSC-CMs

Effects of ACO on APs were measured in ventricular (V)-like hiPSC-CMs which were characterized based on their AP properties including APD, APA and dV/dt_{Max} [18,19,28]. ACO (0.3, 1.0 and 3.0 μM) concentration-dependently increased the BF, shortened APD30, APD50 and ADP90, and reduced APA in hiPSC-CMs while prolonged exposure (180~300 seconds) to a higher concentration of ACO (3.0 μM) led to more remarkable effects including a positively shift of the MDP, increased prevalence of DADs followed by VF-like AP waveforms till their

Table 1. Effects of ACO on action potentials of hiPSC-CMs.

hiPSC-CMs (n = 7)	Baseline	ACO (0.3 μM)	ACO (3 μM)
APA (mV)	110.92 \pm 1.78	103.42 \pm 2.42*	96.31 \pm 1.32 [†]
APD30 (ms)	402.46 \pm 47.98	316.40 \pm 35.60*	199.22 \pm 16.89 [†]
APD50 (ms)	456.03 \pm 50.89	370.81 \pm 38.79*	237.43 \pm 16.92 [†]
APD90 (ms)	520.77 \pm 58.28	436.45 \pm 39.62*	296.42 \pm 16.06 [†]
APD90/APD30	1.305 \pm 0.04	1.401 \pm 0.06	1.518 \pm 0.06 [†]
APD90/APD50	1.14 \pm 0.02	1.19 \pm 0.02 [†]	1.26 \pm 0.03 [†]
MDP (mV)	-62.10 \pm 1.49	-60.75 \pm 1.35	-59.68 \pm 1.14*
Over shoot (mV)	48.82 \pm 1.67	42.67 \pm 2.40*	36.64 \pm 1.78 [†]
BF (beats/min)	48.60 \pm 4.16	67.35 \pm 7.79*	77.83 \pm 8.08*
No. of DAD/5 min	0	13.25 \pm 3.87 [†]	60.16 \pm 4.35 [†]

All the parameters were measured in the ventricular-like hiPSC-CMs exposed to ACO for 120 seconds. APD₃₀, APD₅₀, and APD₉₀, action potential duration at 30%, 50% and 90% of repolarization (APDs are corrected by beating rates). APA, action potential amplitude; MDP, maximal diastolic potential; BF, beating frequency; DAD, delayed after-depolarization. Results are shown as Mean \pm SEM.

* $P < 0.05$

[†] $P < 0.01$

[‡] $P < 0.001$ (vs. baseline).

doi:10.1371/journal.pone.0168435.t001

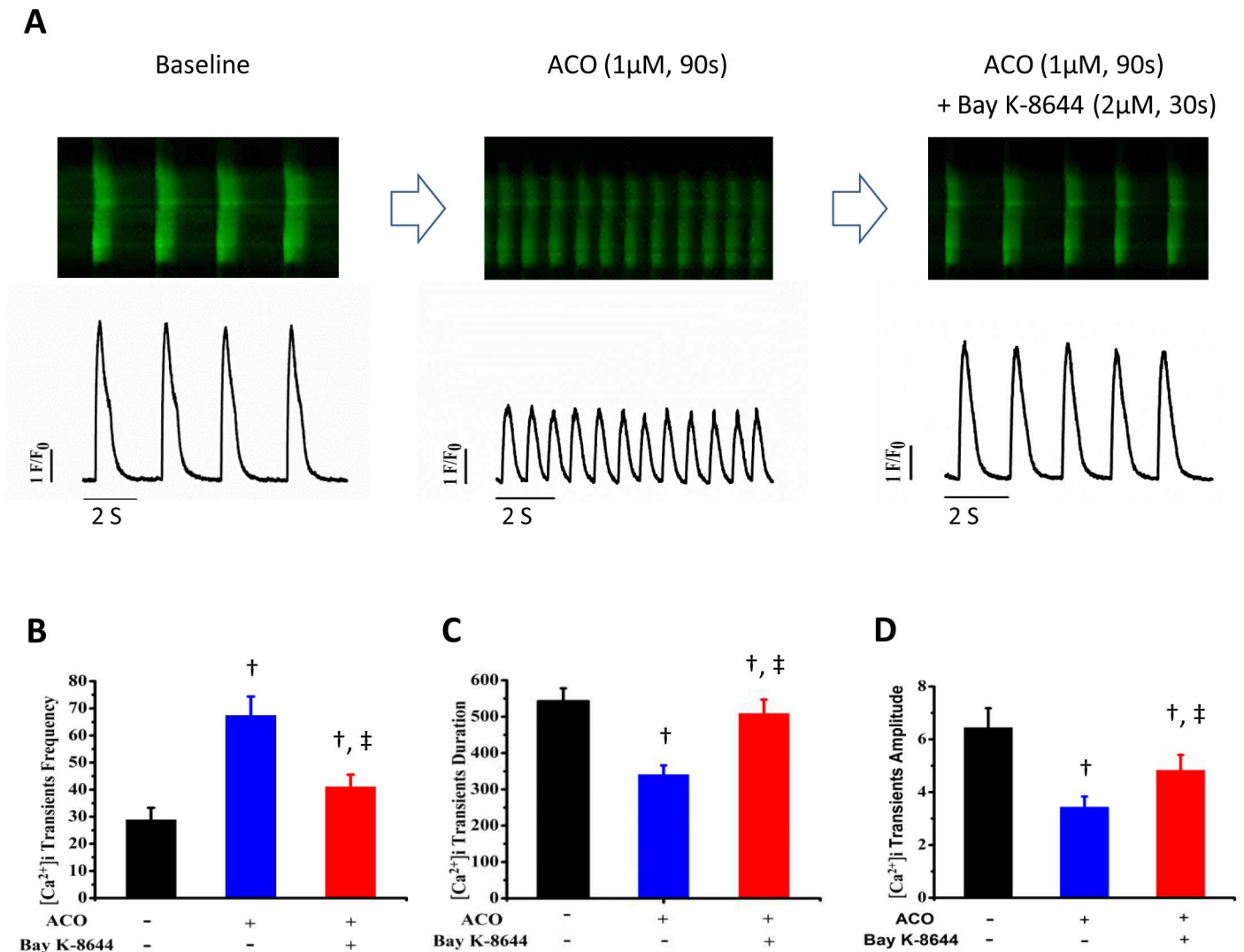


Fig 2. Effects of ACO on [Ca²⁺]_i transients in hiPSC-CMs. (A) Representative traces of the [Ca²⁺]_i transients recorded in a hiPSC-CM at baseline and with subsequent exposure of ACO and ACO plus Bay K-8644. (B, C, and D) Bar-graphs show the changes in [Ca²⁺]_i transient frequency, duration and amplitude in hiPSC-CMs. [†]*p* < 0.01, vs. baseline. [‡]*p* < 0.001, vs. ACO. *n* = 7.

doi:10.1371/journal.pone.0168435.g002

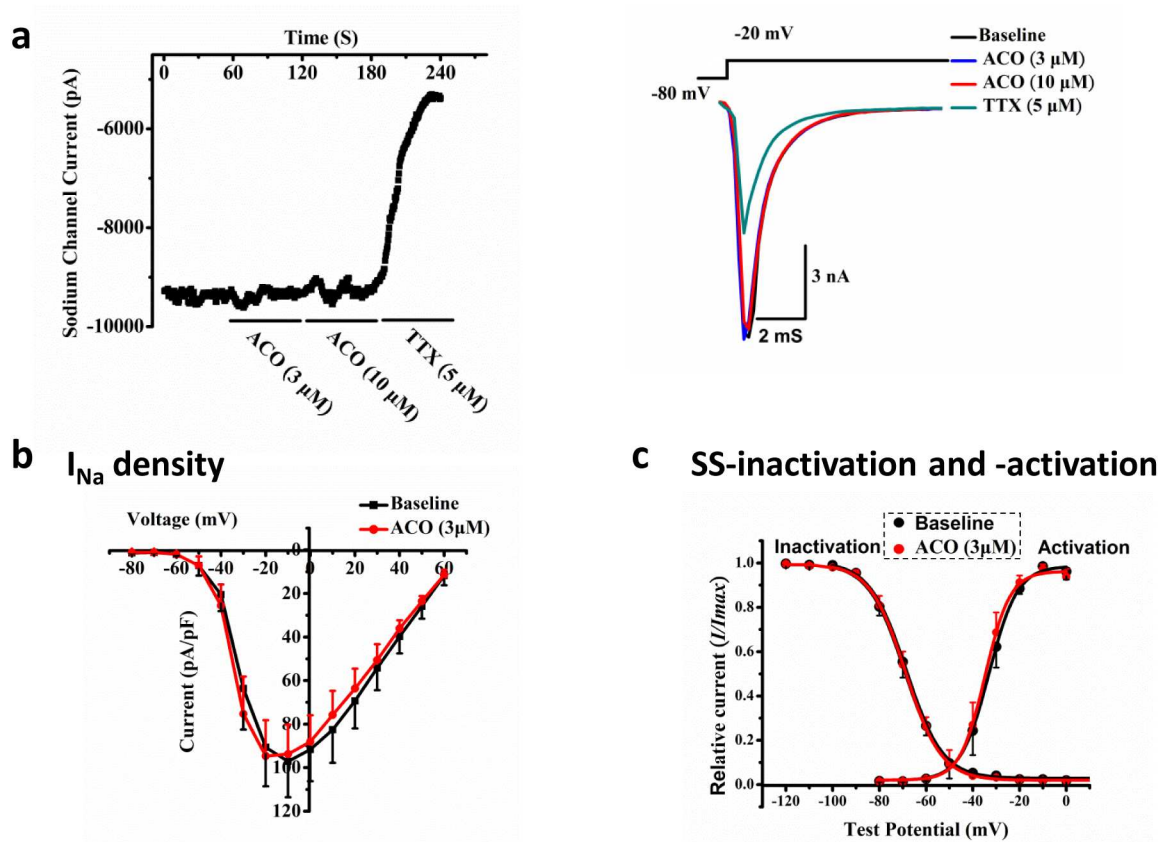
complete diminishment (Fig 1A, Table 1, data for ACO at 1.0 μM not shown). The effects of ACO resembled that of nifedipine, a specific LTCC blocker. Nifedipine (0.3 μM) increased beating frequency, shortened APDs and triggered DADs in hiPSC-CMs followed by a complete abolishing of APs (Fig 1B).

Our data demonstrated nifedipine-like effects of ACO in hiPSC-CMs characterized by shortening of APDs followed by DAD and VF-like changes.

Effects of ACO on [Ca²⁺]_i transients in hiPSC-CMs

In hiPSC-CMs, [Ca²⁺]_i transients reflect calcium-induced calcium release (CICR) triggered by I_{Ca,L} influx [29] and closely correlate with action potentials [30,31]. To validate the nifedipine-

A. Peak I_{Na}



B. Late I_{Na} (I_{NaL})

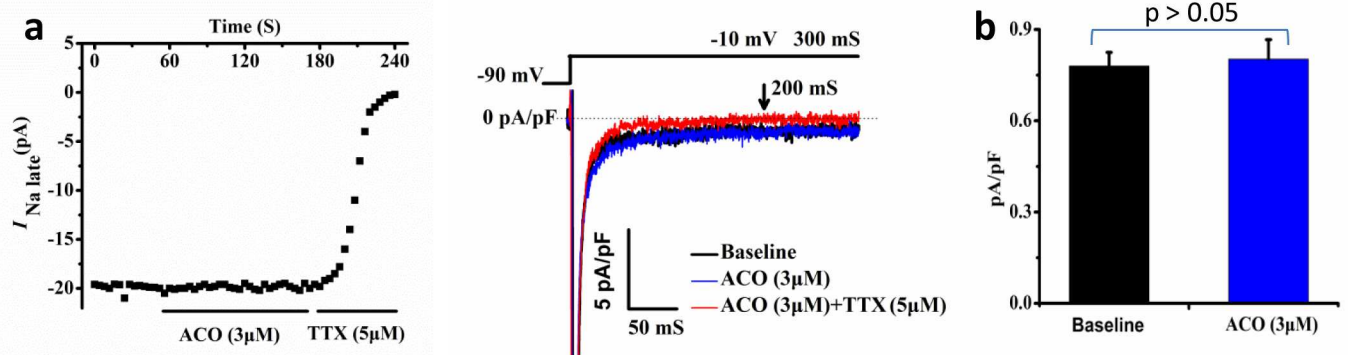


Fig 3. Effects of ACO on sodium currents in hiPSC-CMs. (Aa) A representative time course and corresponding traces of the peak I_{Na} recorded in a hiPSC-CM showing the effect of ACO and TTX. (Ab) The I-V curve showing peak I_{Na} density in hiPSC-CMs. $n = 7$. (Ac) The SS-inactivation and -activation curves. $n = 7$. (Ba) A representative time course and the corresponding traces of late I_{Na} (I_{NaL}) recorded in a hiPSC-CM showing the effects of ACO and TTX. (Bb) A bar-graph showing the average densities of the I_{NaL} (at 200ms) recorded in hiPSC-CMs treated with 3 μ M ACO. $n = 7$.

doi:10.1371/journal.pone.0168435.g003

Table 2. Effect of ACO on SS-activation and -inactivation of I_{Na} in hiPSC-CMs.

		Baseline	ACO (3 μ M)	P value
SS- activation (n = 7)	$V_{1/2}$	-31.13 \pm 1.24	-31.58 \pm 2.36	0.87
	k	4.32 \pm 0.50	4.31 \pm 0.77	0.99
SS- inactivation (n = 7)	$V_{1/2}$	-70.68 \pm 2.03	-70.48 \pm 1.35	0.93
	k	6.66 \pm 0.57	6.40 \pm 0.48	0.74

$V_{1/2}$, half-activation/inactivation voltage. K, slope factor. Results are shown as Mean \pm SEM.

P values were calculated by comparing ACO with baseline.

doi:10.1371/journal.pone.0168435.t002

like effects of ACO on APs, $[Ca^{2+}]_i$ transients were recorded in hiPSC-CMs. ACO at 0.3, 1.0 and 3.0 μ M increased the frequency and decreased the duration and amplitude of $[Ca^{2+}]_i$ transients and such effects were partially abolished by Bay K-8644, a LTCC opener. Fig 2 demonstrates the effects of ACO at 1.0 μ M. Long time (180~300 seconds) exposure of ACO at 3.0 μ M completely abolished the $[Ca^{2+}]_i$ transients (data not shown).

Data from $[Ca^{2+}]_i$ transient assay further consolidated that the effects of ACO on APs are most likely to be achieved through inhibition of LTCC and CICR.

Effects of ACO on I_{Na} and $I_{Ca,L}$ in hiPSC-CMs

Our data of AP and $[Ca^{2+}]_i$ transients indicated that LTCC inhibition by ACO could be a major ionic change in human cardiomyocytes, which is different from the cardiac Na^+ channel activation observed in animal cardiac myocytes. To validate the changes in cardiac ion currents by ACO, I_{Na} and $I_{Ca,L}$ were measured in ACO-treated hiPSC-CMs.

Effects of ACO on I_{Na} in hiPSC-CMs. The peak I_{Na} and late I_{Na} (I_{NaL}) were measured. ACO of up to 10.0 μ M exerted no significant effects on the density of I_{Na} (Fig 3Aa and 3Ab). Neither did ACO alter the SS-activation and -inactivation of I_{Na} (Fig 3Ac, Table 2) which also reflect the window currents. Moreover, ACO failed to alter I_{NaL} (Fig 3B).

Effects of ACO on $I_{Ca,L}$ in hiPSC-CMs. With the “run-down” phenomenon minimized after replacement of extracellular Ca^{2+} with Ba^{2+} , the inhibitory effect of ACO on $I_{Ca,L}$ was confirmed and validated by addition of nifedipine which further blocked $I_{Ca,L}$ (Fig 4A). The inhibitory effect of ACO on LTCC was further validated by addition of Bay K-8644 (1.0 μ M), an $I_{Ca,L}$ opener, which reversed the effect of ACO (Fig 4B). Moreover, a positive shift of the half-activation voltage ($V_{1/2}$) and a negative shift of the $V_{1/2}$ of $I_{Ca,L}$ were observed in hiPSC-CMs treated with ACO while the recovery from inactivation remained unchanged (Fig 4C, 4D and 4E, Table 3). hiPSC-CMs exposed to 0.1 ~ 10.0 μ M of ACO demonstrated a strong concentration-dependent inhibitory effect on $I_{Ca,L}$ with an IC_{50} of 0.68 \pm 0.15 μ M (Fig 4F).

Effects of ACO on I_{Na} , I_{Kr} and $I_{Ca,L}$ recorded in the heterologous expression system

Effects of ACO on major ion currents in hiPSC-CMs were validated in the heterologous expression systems. Using the Patchliner® automated patch-clamping system, effects of ACO (0.01 ~ 100 μ M) on I_{Na} , $I_{Ca,L}$, I_{Kr} were measured in Nav1.5-HEK293, Cav1.2-CHO and hERG-HEK293 cells, respectively. ACO showed milder blockage of I_{Na} and I_{Kr} in Nav1.5-HEK293 and hERG-HEK293 cells with IC_{50} s of 14.1 μ M (n = 14) and 16.0 μ M (n = 19), respectively (Fig 5A and 5B). However, a stronger $I_{Ca,L}$ blocking was noted in Cav1.2-CHO cells exposed to lower concentrations of ACO with IC_{50} of 6.6 μ M (n = 5) (Fig 5C).

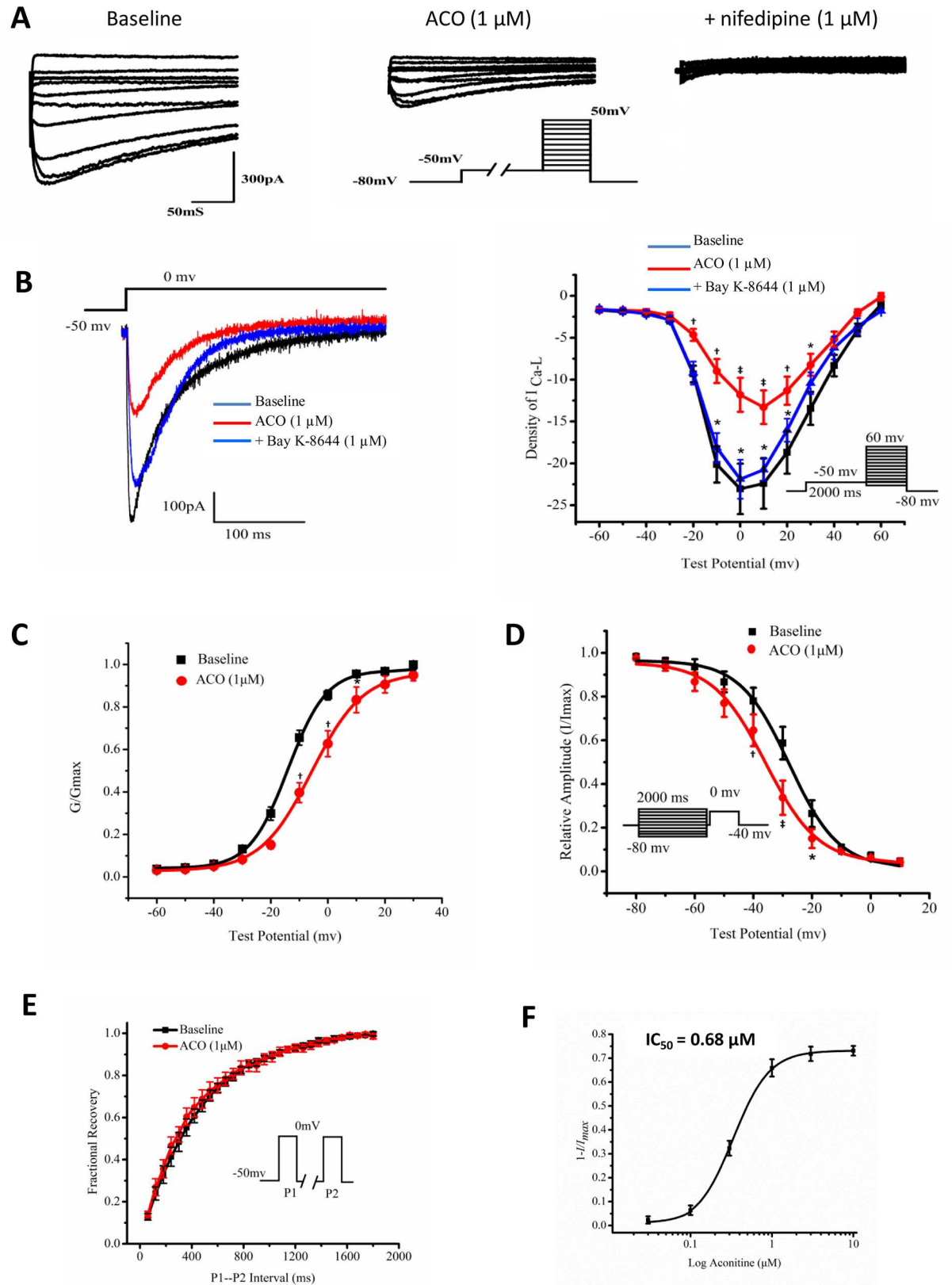


Fig 4. Effects of ACO on $I_{Ca,L}$ in hiPSC-CMs. (A) Representative traces of the voltage-gated LTCC current $I_{Ca,L}$ recorded from a hiPSC-CM at baseline followed by exposure of 1 μ M ACO and addition of 1 μ M nifedipine. (B) Representative traces and I-V curves recorded from hiPSC-CMs exposed to 1 μ M ACO followed by 1 μ M Bay K-8644. * $p < 0.05$, $^{\dagger}p < 0.01$, $^{\ddagger}p < 0.001$, ACO vs. baseline or Bay K-8644 vs ACO, $n = 8$. (C) The voltage-dependent activation curve of $I_{Ca,L}$ recorded in hiPSC-CMs exposed to 1 μ M of ACO. G/G_{max} : normalized peak conductance. * $p < 0.05$, $^{\dagger}p < 0.01$, vs. baseline. $n = 5$. (D) The SS-inactivation curve of $I_{Ca,L}$. * $p < 0.05$, $^{\dagger}p < 0.01$, $^{\ddagger}p < 0.001$, vs. baseline. $n = 5$. (E) Recovery from inactivation of $I_{Ca,L}$. $n = 5$. Insert shows the 2-pulse protocol. (F) The IC_{50} of ACO on $I_{Ca,L}$ ($n = 8$).

doi:10.1371/journal.pone.0168435.g004

Effects of ACO on extracellular field potentials

To validate the potential impact of ACO-induced APD shortening on electrocardiography (ECG), the extracellular field potentials (FP) of hiPSC-CMs were measured using the MEA system which produces signals resemble the ECG. ACO-treated hiPSC-CMs showed a tendency of concentration-dependent increase of BF, decrease of Ca^{2+} wave and shortening of FPDc (Fig 6). Yet the heart rate increments and Ca^{2+} wave reduction were obvious at higher concentrations of ACO while a moderate FPDc shortening was significant at 0.03 and 0.1 μ M of ACO (Fig 6B). Cell contractions were stopped by ACO at higher concentrations and with longer exposure time ($> 3 \mu$ M and > 300 s) (data not shown).

Data from the MEA assay, including the increased BF, decreased Ca^{2+} wave (which echoes $I_{Ca,L}$ inhibition observed with single cells) and shortened FPDc, support our findings in single hiPSC-CM.

Effects of ACO on I_{Na} in isolated Guinea-pig ventricular myocytes

To validate the effect of ACO on sodium currents in hiPSC-CMs, I_{Na} and I_{NaL} were measured in isolated Guinea-pig ventricular myocytes treated with 3 μ M ACO. The peak sodium current densities recorded during -80mV to -50mV significantly increased by ACO while it remained unchanged during -45 mV to +20 mV (Fig 7A and 7B). Moreover, ACO negatively shifted the activation of I_{Na} by 12.58 mV (-47.66 ± 0.71 vs -60.24 ± 2.22) and positively shifted the inactivation of I_{Na} by 4.32 mV (-69.97 ± 1.78 vs -74.29 ± 1.20) (Fig 7C, Table 4) and markedly increased the I_{NaL} at the voltages between -55 and -85 mV (Fig 7D and 7E). Thus, the well-anticipated effect of ACO on opening of the I_{NaL} was validated in Guinea pig cardiac myocytes.

Discussion

In the current study, we observed that ACO, within the well-adopted in vitro doses and closer to the toxicological concentrations, is capable of triggering proarrhythmic effects in human cardiomyocytes characterized by increased beating frequency and shortened repolarization phases of action potentials and field potentials followed by increased prevalence of DADs and cardiac arrest. Such changes were accompanied by reduced duration and amplitude of $[Ca^{2+}]_i$

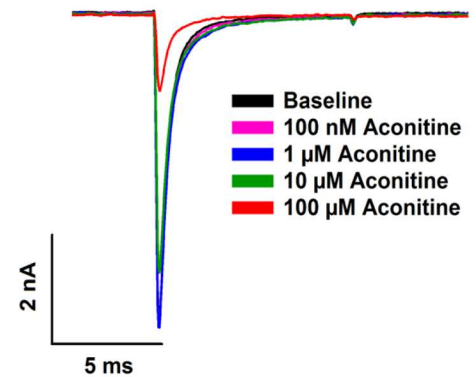
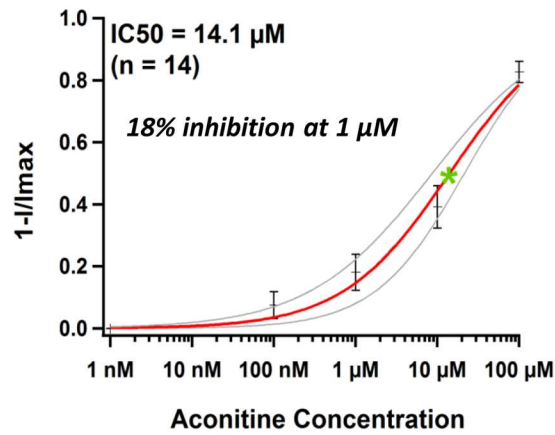
Table 3. Effect of ACO on the kinetics of $I_{Ca,L}$

		Baseline	ACO (1 μ M)	P value
Activation ($n = 8$)	$V_{1/2}$	-13.81 ± 0.69	-5.66 ± 1.27	0.010
	κ	6.94 ± 0.53	8.25 ± 0.72	0.082
SS-inactivation ($n = 8$)	$V_{1/2}$	-27.69 ± 1.43	-34.06 ± 1.69	0.016
	κ	8.94 ± 0.87	10.6 ± 1.02	0.371
Recovery from Inactivation ($n = 5$)	τ	441.45 ± 35.13	413.12 ± 44.99	0.667

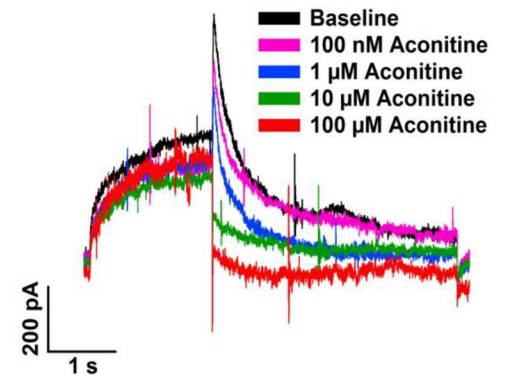
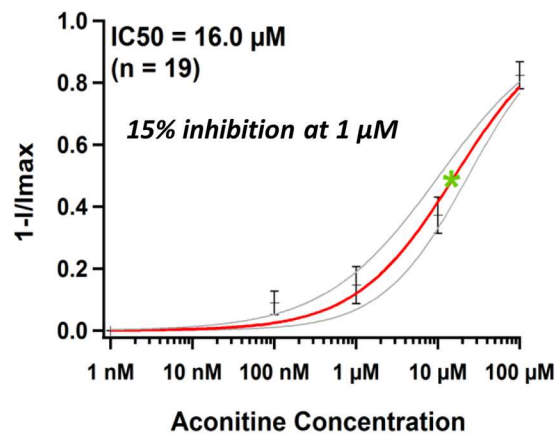
$V_{1/2}$, half-activation/inactivation voltage. κ , slope factor. τ , the recovery time constant. Results are shown as Mean \pm SEM. P values were calculated by comparing ACO with baseline.

doi:10.1371/journal.pone.0168435.t003

A, I_{Na}



**B, I_{kr}
(peak tail)**



C, $I_{Ca,L}$

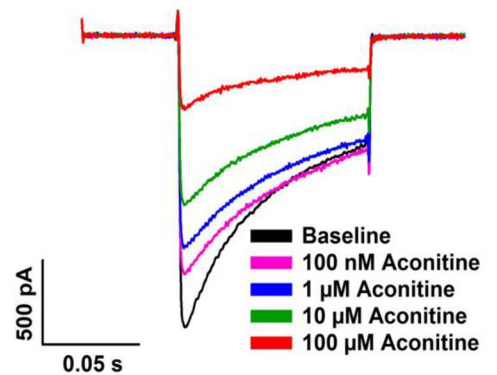
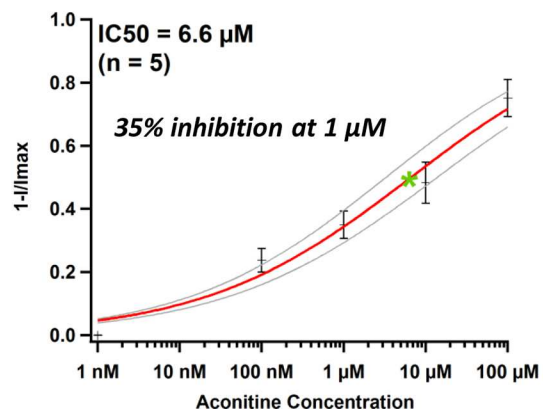


Fig 5. Effects of ACO on I_{Na} , I_{Kr} and $I_{Ca,L}$ in heterologous expression systems. Nav1.5-HEK293, hERG-HEK293 and Cav1.2-CHO cells were exposed to 0.1–100 μ M ACO. (A) The concentration-dependent inhibition curve of I_{Na} and representative traces recorded. (B) The concentration-dependent inhibition curve of I_{Kr} (peak tail: the peak of the tail current) and representative traces. (C) The concentration-dependent inhibition curve of $I_{Ca,L}$ and representative traces.

doi:10.1371/journal.pone.0168435.g005

transients and Ca^{2+} wave. Moreover, data from hiPSC-CMs and the heterologous expression systems directly indicated that ACO could selectively inhibit $I_{Ca,L}$ independent from $[Na^+]_i$ and Na^+ channel activities as the peak, late and window I_{Na} remained unaffected.

ACO has long been known as a neurotoxin that selectively interacts with the voltage-dependent neuronal Na^+ channels by binding to its neurotoxin binding site 2 at the pore region of the alpha subunit, rendering a prolonged opening of the Na^+ channel [32]. In isolated cardiac myocytes of various animals, ACO has been shown to act as an I_{Na} agonist that opens the Na^+ channels during the depolarization/repolarization phases, leading to a delayed repolarization [7–9]. However, our data from human hiPSC-CMs and transgenic cell line (Nav1.5-HEK293), controlled by Guinea-pig ventricular myocytes, minimized the possibility that ACO-increased cytosolic $[Na^+]_i$ in human cardiomyocytes acts as the main driver of cardiac arrhythmia [13,14]. Rather, our data indicate that inhibitions of LTCC and CICR by ACO could play a key role in the proarrhythmic effects of ACO in human and ACO is capable of blocking LTCC following a mechanism independent from increased $[Na^+]_i$. The effects of ACO on cardiac repolarization in hiPSC-CMs resemble that of nifedipine, which, like Bay K-8644, belongs to dihydropyridines, the most selective and potent calcium channel modulators specifically identify LTCC activity in cardiac myocyte [33]. Moreover, the effect of ACO on beating frequency also resemble that of nifedipine that has been shown capable of increasing the BF in cardiomyocytes derived from hiPSCs and human embryonic stem cells [34,35].

Defects in cardiac LTCC have been associated with severe arrhythmias in human. Loss-of-function of cardiac LTCC due to genetic mutations have been associated with inherited J-wave syndromes and sudden cardiac death [36] and short QT syndrome characterized by an abnormally short QT interval and an increased risk of atrial and ventricular fibrillation [25,37]. Decreased $I_{Ca,L}$ has been found in patients with atrial fibrillation [38].

Nevertheless, caution should be exercised to apply the data obtained in hiPSC-CMs to the intact human heart. ECG findings in patients with ACO-induced cardiotoxicity have been explained so far by the persistent activation of Na^+ channels and subsequent accumulation of cytosolic Ca^{2+} . The current study, however, suggests that $I_{Ca,L}$ inhibition plays a key role in the effects of ACO in human cardiomyocytes. We noted that ACO at lower concentrations and shorter exposure time ($< 3 \mu$ M and < 300 s) could rapidly shorten the repolarization phase (APD and FPDc) in hiPSC-CMs while increased dosages and longer exposure time abolished the electrical activities (Figs 2A and 6). In patients with aconitine intoxication, $I_{Ca,L}$ inhibition, rather than I_{Na} activation, may offer a new explanation for atrioventricular blocks and bradycardia, the major ECG defects identified in almost all patients, in addition to the effect of parasympathetic activation, as $I_{Ca,L}$ is the major driver of the depolarization of the pacemaker myocytes. However, data from hiPSC-CMs fall short to explain why QT-shortening has not been found in patients yet QT prolongation has been reported in some patients instead [39]. While the neurohormonal effects of ACO in cardiotoxicity [1] may explain some of the discrepancy between the electrophysiological characteristics of a ventricular myocyte (such as APs) and the heart (such as ECG), a possible role of I_{Kr} inhibition, the doses of ACO and the exposure time/duration might all contribute to the variable cardiac repolarization durations in human heart. Firstly, we recorded a moderate I_{Kr} inhibition in hERG-HEK293 cells treated by ACO which is consistent with previous in vitro studies [16,17]. Under certain conditions, the effects of I_{Kr} inhibition may become dominant over that of $I_{Ca,L}$. Secondly, different species of

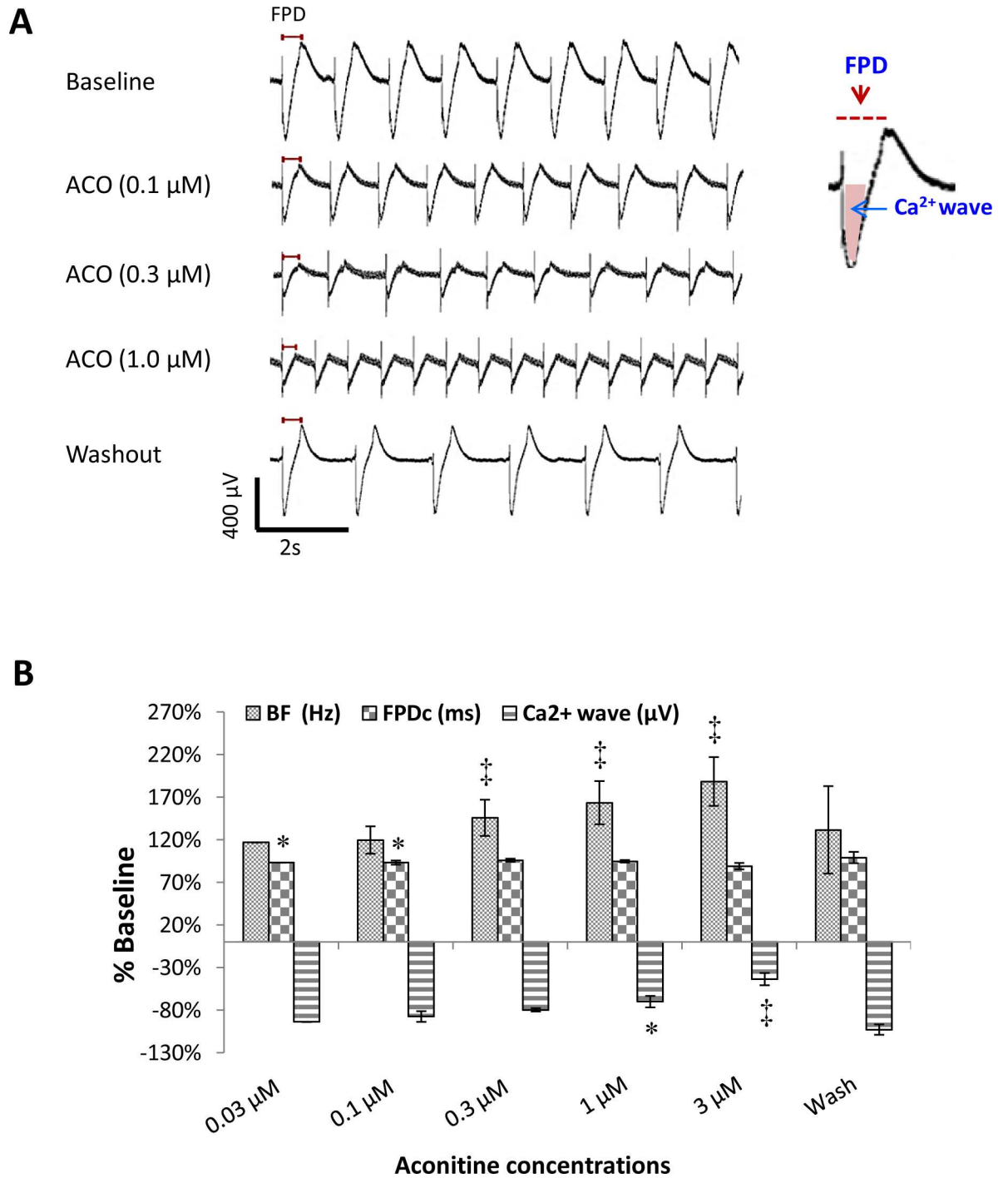


Fig 6. Effects of ACO on the field potentials in hiPSC-CMs. (A) Representative traces of the field potentials (FPD) recorded with a cluster of hiPSC-CMs at baseline, exposed to various concentrations of ACO and after washout. (B) A bar-graph demonstrates the average beating frequency (BF), Ca²⁺ waves and FPDc recorded at baseline, with 0.03, 0.1, 0.3, 1.0 and 3.0 μM of ACO treatments and after washout. **p* < 0.05, †*p* < 0.001; vs. baseline. *n* = 4.

doi:10.1371/journal.pone.0168435.g006

ACO-containing herbs and different ways of administration could contribute to different concentrations of ACO in patients. Lastly, our data from hiPSC-CMs were obtained within 30

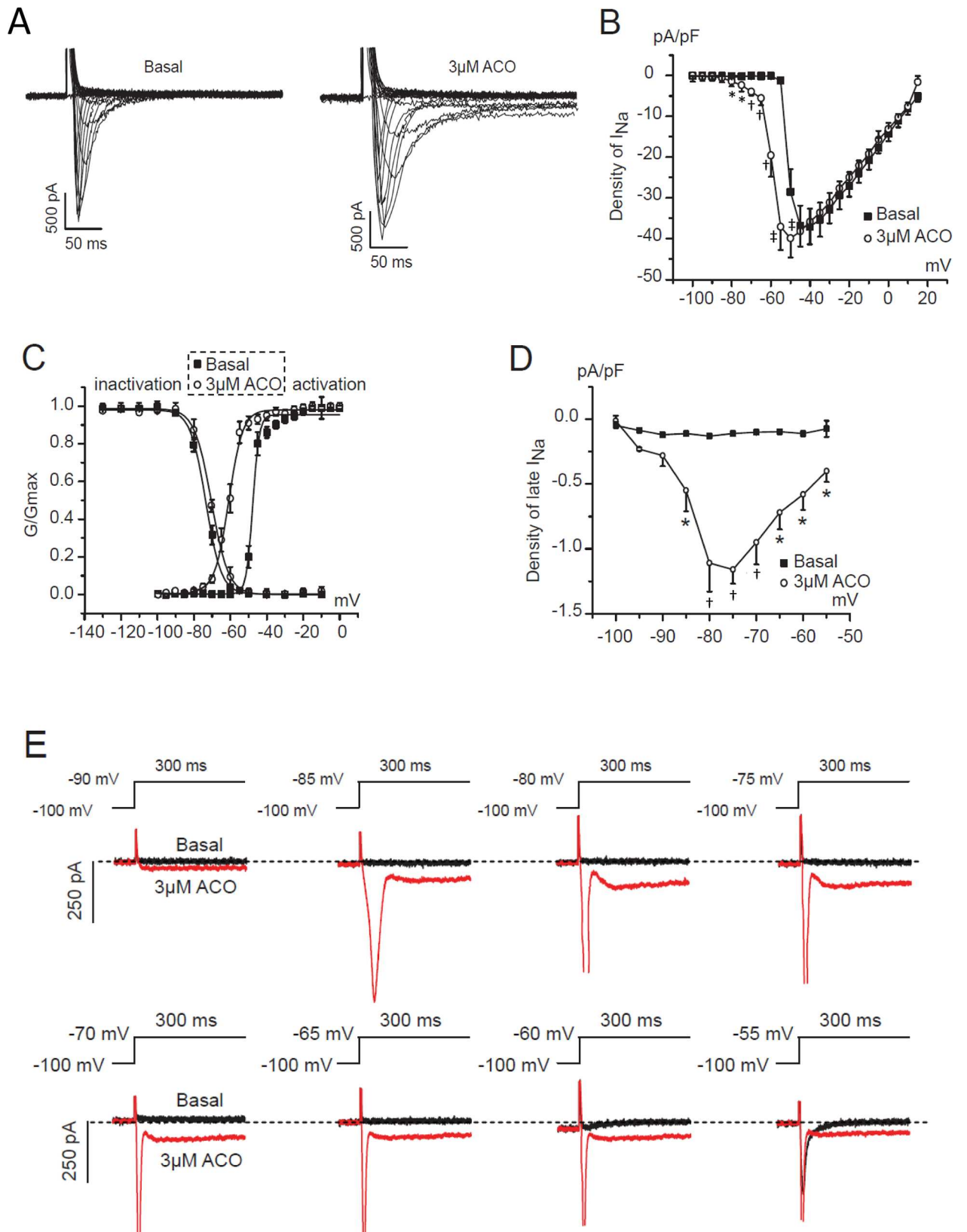


Fig 7. Effects of ACO on sodium currents in Guinea-pig ventricular myocytes. (A) Representative traces of the peak I_{Na} recorded in a Guinea-pig ventricular myocyte prior to and after 3 μ M ACO. (B) The I-V curves showing the current densities of peak I_{Na} . n = 5. (C) The SS-inactivation and -activation curves. n = 5. (D) The I-V curves of the voltage-gated I_{NaL} densities. n = 5. (E) Representative traces of voltage-dependent I_{NaL} recorded in a Guinea-pig ventricular myocyte prior to and post 3 μ M ACO. * $p < 0.05$, † $p < 0.01$, vs. baseline.

doi:10.1371/journal.pone.0168435.g007

Table 4. Effect of ACO on SS-activation and -inactivation of I_{Na} in Guinea-pig ventricular myocytes.

		Baseline	ACO (3 μ M)
SS-activation (n = 5)	$V_{1/2}$	-47.66 \pm 0.71	-60.24 \pm 2.22 [†]
	κ	1.77 \pm 0.38	1.10 \pm 0.094
SS-inactivation (n = 5)	$V_{1/2}$	-69.97 \pm 1.78	-74.29 \pm 1.20*
	κ	4.03 \pm 0.19	3.89 \pm 0.22

$V_{1/2}$, half-activation/inactivation voltage. K, slope factor. Results are shown as Mean \pm SEM.

* $P < 0.05$

† $P < 0.01$ (vs. baseline).

doi:10.1371/journal.pone.0168435.t004

minutes while it takes an average of 4 hours (earliest 2 hours) to have the 1st ECG recorded in patients with ACO ingestions [1], leaving the early change of ECG unchecked.

In addition, our data hint that ACO may also inhibit LTCC in vascular smooth muscle cells and compromise the vascular tone and thus contribute to the severe hypotensive effect in addition to its actions on autonomic nervous system. It is reported that overdose of LTCC inhibitors could cause severe hypotension [40] likely due to reduced vascular tones following the LTCC inhibition in vascular smooth muscle cells [41].

Although blocking of $Kv1.5$ channels and I_{Kur} in ACO-treated neonatal cardiomyocytes have been associated with prolonged APDs and EADs [15,16], such changes are unlikely to happen in human ventricular myocytes and pacemaker cells as I_{Kur} is predominantly expressed in atrial myocytes [42].

Aconitum, along or as an important ingredient in many traditional Chinese medicine prescriptions, will continually be adopted for treating various disease conditions and ACO-induced arrhythmias will remain to be a health threat [1,2]. To date, there is no effective ion channel-targeted therapy for ACO poisoning as sodium channel blockers appeared to be the least effective drugs [1]. Our data may shed new light on more targeted drug therapies.

The current study highlights the importance of applying human cardiomyocyte models for evaluating the effects of various drugs. The identification of a different mechanism of ACO-induced arrhythmia in human cardiomyocytes compared to that from other animals, particularly rodents, highlights the intra-species variations in cardiac electrophysiology [22, 23]. Data of the current and previous studies indicate that the cardiac Na^+ channels of different species could have different sensitive to ACO while the TTX-insensitive Na^+ channels could be insensitive to ACO as a high concentration of ACO (100 μ M) [43] on human Na^+ channels achieved the similar effect of 3 μ M ACO (close to physiological concentrations) on isolated Guinea-pig ventricular myocytes. Whereas lower concentrations of ACO of (3~10 μ M) failed to alter human I_{Na} .

In summary, for the first time we observed the proarrhythmic effects of ACO in human cardiomyocytes and such effects are likely to be achieved via inhibition of LTCC.

Supporting Information

S1 File. Supplemental Methods.

(DOC)

Author Contributions

Conceptualization: HW SS.

Data curation: HW SS.

Formal analysis: JW XW YYC CHK ZL HW SS.

Funding acquisition: HW SS CW.

Investigation: JW XW YYC CHK ZL HG.

Methodology: HW SS JW XW YYC CHK HG.

Resources: HW SS CW.

Software: QY.

Supervision: HW SS CW.

Validation: ZL.

Writing – original draft: HW.

Writing – review & editing: HW JW XW SS.

References

1. Tai YT, But PP, Young K, Lau CP (1992) Cardiotoxicity after accidental herb-induced aconite poisoning. *Lancet* 340: 1254–1256. PMID: [1359321](#)
2. Chan TY (2009) Aconite poisoning. *Clin Toxicol (Phila)* 47: 279–285.
3. Colussi C, Berni R, Rosati J, Straino S, Vitale S, Spallotta F, et al. (2010) The histone deacetylase inhibitor suberoylanilide hydroxamic acid reduces cardiac arrhythmias in dystrophic mice. *Cardiovasc Res* 87: 73–82. doi: [10.1093/cvr/cvq035](#) PMID: [20164117](#)
4. Bartosova L, Novak F, Bebarova M, Frydrych M, Brunclik V, Opatrilova R, et al. (2007) Antiarrhythmic effect of newly synthesized compound 44Bu on model of aconitine-induced arrhythmia—compared to lidocaine. *Eur J Pharmacol* 575: 127–133. doi: [10.1016/j.ejphar.2007.07.044](#) PMID: [17706639](#)
5. Amran MS, Hashimoto K, Homma N (2004) Effects of sodium-calcium exchange inhibitors, KB-R7943 and SEA0400, on aconitine-induced arrhythmias in guinea pigs in vivo, in vitro, and in computer simulation studies. *J Pharmacol Exp Ther* 310: 83–89. doi: [10.1124/jpet.104.066951](#) PMID: [15028781](#)
6. Ohno Y, Chiba S, Uchigasaki S, Uchima E, Nagamori H, Mizugaki M, et al. (1992) The influence of tetrodotoxin on the toxic effects of aconitine in vivo. *Tohoku J Exp Med* 167: 155–158. PMID: [1475787](#)
7. Peper K, Trautwein W (1967) The effect of aconitine on the membrane current in cardiac muscle. *Pflügers Archiv für die gesamte Physiologie des Menschen und der Tiere* 296: 328–36.
8. Nilius B, Boldt W, Benndorf K (1986) Properties of aconitine-modified sodium channels in single cells of mouse ventricular myocardium. *Gen Physiol Biophys* 5: 473–484. PMID: [2433183](#)
9. Honerjager P, Meissner A (1983) The positive inotropic effect of aconitine. *Naunyn Schmiedeberg's Arch Pharmacol* 322: 49–58. PMID: [6302523](#)
10. Liu QH, Li XL, Xu YW, Lin YY, Cao JM, Wu BW (2012) A novel discovery of IK1 channel agonist: zacopride selectively enhances IK1 current and suppresses triggered arrhythmias in the rat. *J Cardiovasc Pharmacol* 59: 37–48 doi: [10.1097/FJC.0b013e3182350bcc](#) PMID: [21921806](#)
11. Fu M, Li RX, Fan L, He GW, Thornburg KL, Wang Z. (2008) Sarcoplasmic reticulum Ca²⁺ release channel ryanodine receptor (RyR2) plays a crucial role in aconitine-induced arrhythmias. *Biochem Pharmacol* 75: 2147–2156. doi: [10.1016/j.bcp.2008.02.027](#) PMID: [18439986](#)
12. Chen L, Ma C, Cai BC, Lu YM, Wu H (1995) [Single channel analysis of aconitine blockade of calcium channels in rat myocardiocytes]. *Yao Xue Xue Bao* 30: 168–171. PMID: [7543723](#)
13. Findlay I (2004) Physiological modulation of inactivation in L-type Ca²⁺ channels: one switch. *J Physiol* 554: 275–283 doi: [10.1113/jphysiol.2003.047902](#) PMID: [12824441](#)
14. Hancox JC, Levi AJ (1996) Actions of the digitalis analogue strophanthidin on action potentials and L-type calcium current in single cells isolated from the rabbit atrioventricular node. *Br J Pharmacol* 118:1447–1454. PMID: [8832071](#)

15. Wang YJ, Chen BS, Lin MW, Lin AA, Peng H, Sung RJ, et al. (2008) Time-dependent block of ultra-rapid-delayed rectifier K⁺ currents by aconitine, a potent cardiotoxin, in heart-derived H9c2 myoblasts and in neonatal rat ventricular myocytes. *Toxicol Sci* 106: 454–463. doi: [10.1093/toxsci/kfn189](https://doi.org/10.1093/toxsci/kfn189) PMID: [18779382](https://pubmed.ncbi.nlm.nih.gov/18779382/)
16. Li Y, Tu D, Xiao H, Du Y, Zou A, Liao Y, et al. (2010) Aconitine blocks HERG and Kv1.5 potassium channels. *J Ethnopharmacol* 131: 187–195. doi: [10.1016/j.jep.2010.06.025](https://doi.org/10.1016/j.jep.2010.06.025) PMID: [20600762](https://pubmed.ncbi.nlm.nih.gov/20600762/)
17. Xie S, Jia Y, Liu A, Dai R, Huang L (2015) Hypaconitine-induced QT prolongation mediated through inhibition of KCNH2 (hERG) potassium channels in conscious dogs. *J Ethnopharmacol* 166: 375–379. doi: [10.1016/j.jep.2015.03.023](https://doi.org/10.1016/j.jep.2015.03.023) PMID: [25800797](https://pubmed.ncbi.nlm.nih.gov/25800797/)
18. Moretti A, Bellin M, Welling A, Jung CB, Lam JT, Bott-Flügel L, et al. (2010) Patient-specific induced pluripotent stem-cell models for long-QT syndrome. *N Engl J Med* 363: 1397–1409. doi: [10.1056/NEJMoa0908679](https://doi.org/10.1056/NEJMoa0908679) PMID: [20660394](https://pubmed.ncbi.nlm.nih.gov/20660394/)
19. Ma D, Wei H, Zhao Y, Lu J, Li G, Sahib NB, et al. (2013) Modeling type 3 long QT syndrome with cardiomyocytes derived from patient-specific induced pluripotent stem cells. *Int J Cardiol* 168: 5277–5286. doi: [10.1016/j.ijcard.2013.08.015](https://doi.org/10.1016/j.ijcard.2013.08.015) PMID: [23998552](https://pubmed.ncbi.nlm.nih.gov/23998552/)
20. Liang P, Lan F, Lee AS, Gong T, Sanchez-Freire V, Wang Y, et al. (2013) Drug screening using a library of human induced pluripotent stem cell-derived cardiomyocytes reveals disease-specific patterns of cardiotoxicity. *Circulation* 127: 1677–1691. doi: [10.1161/CIRCULATIONAHA.113.001883](https://doi.org/10.1161/CIRCULATIONAHA.113.001883) PMID: [23519760](https://pubmed.ncbi.nlm.nih.gov/23519760/)
21. Lu J, Wei H, Wu J, Jamil MF, Tan ML, Adenan MI, et al. (2014) Evaluation of the cardiotoxicity of mitragynine and its analogues using human induced pluripotent stem cell-derived cardiomyocytes. *PLoS One* 9: e115648 doi: [10.1371/journal.pone.0115648](https://doi.org/10.1371/journal.pone.0115648) PMID: [25535742](https://pubmed.ncbi.nlm.nih.gov/25535742/)
22. Linz KW, Meyer R (2000) Profile and kinetics of I-type calcium current during the cardiac ventricular action potential compared in guinea-pigs, rats and rabbits. *Pflugers Arch* 439: 588–599.
23. O'Hara T, Rudy Y (2012) Quantitative comparison of cardiac ventricular myocyte electrophysiology and response to drugs in human and nonhuman species. *Am J Physiol Heart Circ Physiol* 302: H1023–1030. doi: [10.1152/ajpheart.00785.2011](https://doi.org/10.1152/ajpheart.00785.2011) PMID: [22159993](https://pubmed.ncbi.nlm.nih.gov/22159993/)
24. Clements M, Thomas N (2014) High-throughput multi-parameter profiling of electrophysiological drug effects in human embryonic stem cell derived cardiomyocytes using multi-electrode arrays. *Toxicol Sci* 140: 445–461. doi: [10.1093/toxsci/ktu084](https://doi.org/10.1093/toxsci/ktu084) PMID: [24812011](https://pubmed.ncbi.nlm.nih.gov/24812011/)
25. Templin C, Ghadri JR, Rougier JS, Baumer A, Kaplan V, Albesa M, et al. (2011) Identification of a novel loss-of-function calcium channel gene mutation in short QT syndrome (SQTS6). *Eur Heart J* 32: 1077–1088. doi: [10.1093/eurheartj/ehr076](https://doi.org/10.1093/eurheartj/ehr076) PMID: [21383000](https://pubmed.ncbi.nlm.nih.gov/21383000/)
26. Rajamohan D, Kalra S, Duc Hoang M, George V, Staniforth A, Russell H, et al. (2016) Automated Electrophysiological and Pharmacological Evaluation of Human Pluripotent Stem Cell-Derived Cardiomyocytes. *Stem Cells Dev* 25: 439–452. doi: [10.1089/scd.2015.0253](https://doi.org/10.1089/scd.2015.0253) PMID: [26906236](https://pubmed.ncbi.nlm.nih.gov/26906236/)
27. Niitsu H, Fujita Y, Fujita S, Kumagai R, Takamiya M, Aoki Y, et al. (2013) Distribution of Aconitum alkaloids in autopsy cases of aconite poisoning. *Forensic Sci Int* 227: 111–117. doi: [10.1016/j.forsciint.2012.10.021](https://doi.org/10.1016/j.forsciint.2012.10.021) PMID: [23131306](https://pubmed.ncbi.nlm.nih.gov/23131306/)
28. Ma J, Guo L, Fiene SJ, Anson BD, Thomson JA, Kamp TJ, et al. (2011) High purity human-induced pluripotent stem cell-derived cardiomyocytes: electrophysiological properties of action potentials and ionic currents. *Am J Physiol Heart Circ Physiol* 301: H2006–2017. doi: [10.1152/ajpheart.00694.2011](https://doi.org/10.1152/ajpheart.00694.2011) PMID: [21890694](https://pubmed.ncbi.nlm.nih.gov/21890694/)
29. Zhang GQ, Wei H, Lu J, Wong P, Shim W (2013) Identification and characterization of calcium sparks in cardiomyocytes derived from human induced pluripotent stem cells. *PLoS One* 8: e55266. doi: [10.1371/journal.pone.0055266](https://doi.org/10.1371/journal.pone.0055266) PMID: [23408964](https://pubmed.ncbi.nlm.nih.gov/23408964/)
30. Spencer CI, Baba S, Nakamura K, Hua EA, Sears MA, Fu CC, et al. (2014) Calcium transients closely reflect prolonged action potentials in iPSC models of inherited cardiac arrhythmia. *Stem Cell Reports* 3: 269–281. doi: [10.1016/j.stemcr.2014.06.003](https://doi.org/10.1016/j.stemcr.2014.06.003) PMID: [25254341](https://pubmed.ncbi.nlm.nih.gov/25254341/)
31. Kim JJ, Yang L, Lin B, Zhu X, Sun B, Kaplan AD, et al. (2015) Mechanism of automaticity in cardiomyocytes derived from human induced pluripotent stem cells. *J Mol Cell Cardiol* 81: 81–93. doi: [10.1016/j.yjmcc.2015.01.013](https://doi.org/10.1016/j.yjmcc.2015.01.013) PMID: [25644533](https://pubmed.ncbi.nlm.nih.gov/25644533/)
32. Rao S, Sikdar SK (2000) Modification of alpha subunit of RIIA sodium channels by aconitine. *Pflugers Arch* 439: 349–355. PMID: [10650987](https://pubmed.ncbi.nlm.nih.gov/10650987/)
33. Bers DM, Perez-Reyes E (1999) Ca channels in cardiac myocytes: structure and function in Ca influx and intracellular Ca release. *Cardiovasc Res* 42: 339–360. PMID: [10533572](https://pubmed.ncbi.nlm.nih.gov/10533572/)
34. Sheng X, Reppel M, Nguemo F, Mohammad FI, Kuzmenkin A, Hescheler J, et al. (2012) Human pluripotent stem cell-derived cardiomyocytes: response to TTX and lidocaine reveals strong cell to cell variability. *PLoS One* 7: e45963. doi: [10.1371/journal.pone.0045963](https://doi.org/10.1371/journal.pone.0045963) PMID: [23029342](https://pubmed.ncbi.nlm.nih.gov/23029342/)

35. Harris K, Aylott M, Cui Y, Louttit JB, McMahon NC, Sridhar A (2013) Comparison of electrophysiological data from human-induced pluripotent stem cell-derived cardiomyocytes to functional preclinical safety assays. *Toxicol Sci* 134: 412–426. doi: [10.1093/toxsci/kft113](https://doi.org/10.1093/toxsci/kft113) PMID: [23690542](https://pubmed.ncbi.nlm.nih.gov/23690542/)
36. Burashnikov E, Pfeiffer R, Barajas-Martinez H, Delpon E, Hu D, Desai M, et al. (2010) Mutations in the cardiac L-type calcium channel associated with inherited J-wave syndromes and sudden cardiac death. *Heart Rhythm* 7: 1872–1882. doi: [10.1016/j.hrthm.2010.08.026](https://doi.org/10.1016/j.hrthm.2010.08.026) PMID: [20817017](https://pubmed.ncbi.nlm.nih.gov/20817017/)
37. Antzelevitch C, Pollevick GD, Cordeiro JM, Casis O, Sanguinetti MC, Aizawa Y, et al. (2007) Loss-of-function mutations in the cardiac calcium channel underlie a new clinical entity characterized by ST-segment elevation, short QT intervals, and sudden cardiac death. *Circulation* 115: 442–449. doi: [10.1161/CIRCULATIONAHA.106.668392](https://doi.org/10.1161/CIRCULATIONAHA.106.668392) PMID: [17224476](https://pubmed.ncbi.nlm.nih.gov/17224476/)
38. Van Wagoner DR, Pond AL, Lamorgese M, Rossie SS, McCarthy PM, Nerbonne JM (1999) Atrial L-type Ca²⁺ currents and human atrial fibrillation. *Circ Res* 85: 428–436. PMID: [10473672](https://pubmed.ncbi.nlm.nih.gov/10473672/)
39. Kim TK, Jin SC, Kim SJ, Choi WI (2013) Analysis of QTc Prolongation Related to Arrhythmia in Patients with Aconitine Intoxication. *Journal of The Korean Society of Emergency Medicine* 24: 548–556.
40. Belson MG, Gorman SE, Sullivan K, Geller RJ (2000) Calcium channel blocker ingestions in children. *Am J Emerg Med* 18: 581–586. doi: [10.1053/ajem.2000.9264](https://doi.org/10.1053/ajem.2000.9264) PMID: [10999574](https://pubmed.ncbi.nlm.nih.gov/10999574/)
41. Zhao Q, Zhao KS (2007) Inhibition of L-type calcium channels in arteriolar smooth muscle cells is involved in the pathogenesis of vascular hyporeactivity in severe shock. *Shock* 28: 717–721. doi: [10.1097/SHK.0b013e318050c914](https://doi.org/10.1097/SHK.0b013e318050c914) PMID: [17607159](https://pubmed.ncbi.nlm.nih.gov/17607159/)
42. Ravens U, Wettwer E (2011) Ultra-rapid delayed rectifier channels: molecular basis and therapeutic implications. *Cardiovasc Res* 89: 776–785. doi: [10.1093/cvr/cvq398](https://doi.org/10.1093/cvr/cvq398) PMID: [21159668](https://pubmed.ncbi.nlm.nih.gov/21159668/)
43. Wright SN (2002) Comparison of aconitine-modified human heart (hH1) and rat skeletal (μ 1) muscle Na⁺ channels: an important role for external Na⁺ ions. *J Physiol* 538: 759–71. doi: [10.1113/jphysiol.2001.012915](https://doi.org/10.1113/jphysiol.2001.012915) PMID: [11826163](https://pubmed.ncbi.nlm.nih.gov/11826163/)